Title

Spatial structures and interaction of multiple sheared flow populations in tokamak edge turbulence

Journal

Nuclear Fusion, 53(8)

ISSN

0029-5515

Authors

Zhao, KJ
Dong, JQ
Yan, LW
et al.

Publication Date

2013-08-01

DOI

10.1088/0029-5515/53/8/083011

Peer reviewed

Spatial structures and interaction of multiple sheared flow populations in tokamak edge turbulence

K. J. Zhao[1,2,3], J. Q. Dong[2,4], L. W. Yan[2], P. H. Diamond [1,5], J. Cheng[2] , W. Y. Hong[2], Z. H. Huang[2] , M. Xu[5], G. R. Tynan[5], K. Itoh[6], S. I. Itoh[7], A. Fujisawa[7], Y. Nagashima[7], S. Inagaki[7], , Z. X. Wang[8], L. Wei[8], Q. Li[2], X. Q. Ji[2], Y. Huang[2], Yi. Liu[2], J. Zhou[2], X. M. Song[2], Q. W. Yang[2], X. T. Ding[2], X. R. Duan[2] and HL-2A team

1. WCI center for fusion theory, NFRI, Gwahangno 113, Yusung-gu, Daejeon 305-806, Korea
2. Southwestern Institute of Physics, P.O. Box 432, Chengdu, China
3. National Fusion Research Institute, Gwahangno 113, Yusung-gu, Daejeon 305-806, Korea
4. Institute for Fusion Theory and Simulation, Zhejiang University, Hangzhou, China,
5. Center for Momentum Transport and Flow Organization, University of California at San Diego, California 92093, USA
6. National Institute for Fusion Science, Toki 509-5292, Japan,
7. Research Institute for Applied mechanics, Kyushu University, Kasuga, Kasuga koen 6-1, 816-8580, Japan
8. School of Physics and Optoelectronic Technology, Dalian University of Technology, Dalian 116024

The radial structures of multiple sheared flow populations and fluctuations were simultaneously measured using combinations of Langmuir probe arrays in the edge plasmas of the HL-2A tokamak with ohmic and electron cyclotron resonance heating (ECRH). The maximum of geodesic acoustic mode (GAM) amplitude locates at ~2-3 cm inside the last close flux surface (LCFS). The low frequency zonal flow (LFZF) and GAM tend to coexist in the inner region. The dependences of the amplitudes of the multiple sheared flows and turbulence on ECRH heating power are also investigated. The measured turbulent Reynolds

stresses are shown to be strongly correlated with the sheared flows, as predicted by theory. The turbulence is modulated at the each frequency of the multiple sheared flows simultaneously, and the particle fluxes induced by the turbulence are significantly reduced near the last close flux surface and in the GAM peaking region. The analyses also show that the spatial structures of the turbulent envelopes at the LFZF and GAM frequencies are similar to those observed in LFZF and GAM.

1. Introduction

Formation of meso- and large-scale structures such as zonal flows (ZFs) is universal in nature such as magnetically confined laboratory and space plasmas, as well as stellar atmospheres. Extensive studies on the structures have been carried out in magnetically confined fusion plasmas to understand the nonlinear processes responsible for the generation of these structures and the resulting reduction of anomalous cross-field transport induced by the turbulent fluctuations.

It is widely accepted in recent decades that small scale-length ambient turbulence (AT) and turbulent transport are reduced or even suppressed by **E**x**B** velocity sheared flows, such as mean flows and ZFs [1-3]. On the other hand, turbulence nonlinear interaction through Reynolds stress contributes to sheared flow formation. This means that there is a feedback loop by which a turbulence-sheared flow system regulates and organizes itself [4-5]. This dynamics involving strong coupling of drift-Rossby waves with zonal flows has also been discussed in geophysical fluid dynamics on the context of a new regime called zonosrtophic turbulence [6].

The ZFs in magnetically confined plasmas are defined as azimuthally symmetric radial electric field fluctuations with finite meso scale radial wavelength ~ L in the regime of $\Delta r_c < L < a$. Here, Δr_c and a are the correlation length of AT and macro scale of the system, respectively. Two types of ZFs in toroidal plasmas have been identified, namely the low frequency zonal flows (LFZFs) [7-8] and the geodesic acoustic modes (GAMs) [9-10] of frequency, $\omega_{GAM} = \sqrt{\gamma(T_i + T_e)/M_i}/R$, where γ is the adiabatic index, T_i and T_e are ion and electron temperature, respectively, M_i and R are ion mass and major radius of the torus,

respectively. Both LFZFs and GAMs have been extensively investigated in recent years [10-22]. The nonlinear interaction between the ZF and AT has also been studied with bicoherence analysis [23]. The direct measurements of nonlinear energy transfer among LFZFs, GAMs and turbulence shows that the kinetic energy is transferred from turbulence into LFZFs and GAMs [24-25]. The correlation measurements between mean flows and turbulence stresses suggest that the sheared flows are driven by turbulence stresses [26-28]. Some experiments suggest that LFZFs or mean flows contribute to transport barrier formation and low to high confinement mode (L-H) transition [29-34]. Nevertheless, the radial structures of multiple sheared flows and turbulence have not been measured when they coexist. The effects of the multiple sheared flows on turbulence have not been detected simultaneously while the LFZFs coexist with GAMs.

The remainder of this work is organized as follows. The experiment set up is given in section 2. The experiment results, including the spatial structures of multiple sheared flows and turbulence, the dynamics, the effects of multiple sheared flows on turbulence and so on, are described in section 3. The conclusions of this work are presented in section 4.

2. Experiment setup

The experiments presented here were conducted in ohmic and ECRH deuterium plasma of the HL-2A tokamak with the major and minor radii of R=1.65m and a=0.4m, respectively. The parameters specially set for the experiments are, the toroidal magnetic field B_t = ~1.3-2.4 T, the plasma current I_p ~150-300 kA, the line average electron density $N_e \approx 1-2.5\times10^{19} m^{-3}$, the safety factor q_{95} ~3.2-4.3. On the HL-2A tokamak, two reciprocating probe systems were set up in the low field side at two toroidal positions with distance ~2100mm. In the experiment, several combinations of distributed Langmuir probe (LP) arrays were used to measure floating-potential and density fluctuations. The first combination is shown in figure.1. A two- step LP arrays of 3 tips and a standard 4 tip array form one fast reciprocating probe set with 65mm poloidal span were used to obtain the distributions of turbulence Reynolds stress, density, and temperature. A radial rake probe array of 12 tips was mounted on another fast reciprocating probe system to detect the radial profiles of the potential fluctuations, radial

electric field. Both fast reciprocating probe sets can be used as the fixed probes. In the second combination, two three-step LP arrays of 6 tips each were utilized to get turbulence Reynolds stress [11]. In addition, a three-step LP array and a Mach probe array form a fast reciprocating probe set of 10 tips with a 65 mm poloidal span. These are used to get the profiles of the poloidal Mach numbers, plasma density and temperature, turbulence stresses. In this combination, the radial rake probe array of 12 tips was also used to measure the distribution of potential fluctuations. The tip size, the data sampling rate and the frequency resolution are the same as in Ref. [11, 14]. The probes are inserted in the edge plasma and the plasma parameters, such as density, temperature, do not change significantly.

3. Experiment results

3. 1. Spatial structure of LFZFs, GAMs and AT

Figure 2 (a) shows the typical auto-power spectra of the floating-potential fluctuations at the radial positions of Δr=-2.4, -2.0, -1.6, and -1.0 cm in ohmic plasmas with edge safety factor of q_{95}=4.0, where the minus sign means inwards from the LCFS. The floating-potential fluctuations are of absolute signals (voltages) and are not normalized. Two distinct features in the spectra are a large power fraction in the frequency range lower than ~5 kHz and a sharp peak at f~12-18 kHz, which were identified as LFZFs and GAMs through measuring the toroidal mode number of n=0 as described in Refs. [11, 14], respectively. The rest is small scale-length AT. The intensity of LFZF and AT increases inwards. The GAM power has a maximum at the position Δr~-2.0 cm and decay inwards. The GAM frequency increases from 12 to 18 kHz inwards, as expected from theory. The amplitude developments of LFZFs, GAMs and AT are examined at the radial position of Δr~-1.2cm further by ECRH power scan of 0, 400, 700 and 1100kW as shown in Figure 2 (b). The intensities of the LFZF and the AT increase with ECRH power. But the GAM peaked at 700kW decays with strong ECRH heating of 1100kW. The GAM decay with strong heating power is consistent with the previous observation which demonstrated that the energy transfer from turbulence into LFZF and GAM increased and decreased, respectively, as the heating power was increased, [25].

The power partition among the LFZF, the GAM and the AT measured by radial rake probe arrays, depending on the local plasma parameters and influencing transport phenomena,

is estimated as a function of radial position. In this analysis, the power partitions of the zonal flows and the turbulence are defined as P_{LFZF}/P_{total}, P_{GAM}/P_{total}, and P_{AT}/P_{total}, respectively. Here, $P_{total}=P_{LFZF}+P_{GAM}+P_{AT}$, and P_{LFZF}, P_{GAM}, and P_{AT} are the LFZF, GAM, and AT power, respectively. In addition, the power is defined as $P=\langle\phi_f^2\rangle$, where ϕ_f^2 is the floating potential fluctuations. Figures 3 (a)-(d) show the radial distributions of the power partitions of the LFZF, GAM, LFZF+GAM and AT in Ohmic (the light lines) and ECRH (the heavy lines) plasmas, respectively. The ECRH power is 300kW. The LFZF power fraction first slightly increases at radial positions from Δr =-0.8 to -3.0 cm, then sharply rises up at Δr=-3.0 to -3.7 cm. In contrast, the power fraction of the GAM sharply increases first from Δr =-0.8 to -1.7 cm, and reaches a maximum at the position of Δr =-1.7 cm, then rapidly decreases at positions from Δr =-1.7 to -3.0 cm.

The GAM power fraction is much higher than that of the LFZF in the radial region of Δr =-0.8 to -2.5 cm, while the power fractions of LFZFs and GAMs are approximately equal from Δr=-3.0 to -3.7 cm. This analysis clearly shows that the LFZF and GAM equally coexist in the inner region while the GAM dominates near the position of ~1.7 cm at the L-mode condition of heating power $P<<P_{th}$. Here, P_{th} is the power threshold to access H-mode plasma. The total power fraction of LFZFs and GAMs is opposite to the AT and is similar in both OH and ECRH cases. The power fraction of LFZFs and GAMs decreases with ECRH power, while that of AT is the opposite. This may have some correlation with the fact that the confinement degrades from OH- to L-mode plasmas.

The radial structures of the multiple sheared flows and AT are studied further in Ohmic and ECRH plasmas with safety factor of q_{95}=3.3. The ECRH power is 500kW. Figures 4 (a) and (b) show the radial electric fields E_r for the LFZF and GAM detected by radial rake probe arrays in Ohmic (light lines) and ECRH (the heavy lines) plasma, respectively. The radial electric fields E_r for the LFZF and GAM were obtained by averaging the absolute E_r amplitudes in the LFZF frequency band of 0.5-4kHz and in GAM the frequency band of 12-18 kHz, respectively. The radial distributions of LFZFs and GAMs are roughly similar to those observed in their power intensity shown Figure 2 (a). However, the maximum of the GAM amplitudes moves inward and locates at Δr~-3.2 cm. The mean flow is also studied by

measuring the poloidal Mach number using probe scan. Figure 4 (c) gives the poloidal Mach number profile. The mean flow velocity is proportion to the Mach number, $\overline{V_\theta} \sim M_{pol} C_s$ where $\overline{V_\theta}$, M_{pol} and C_s are the mean flow velocity, Mach number and ion sound speed, respectively. The Mach numbers in Ohmic and ECRH plasmas have maximums at Δr~-1.0 cm, then decreases inward. The profile of turbulence intensity $\langle \phi^2 \rangle$ at the frequency region of ~30-400 kHz is plotted in Figure 4 (d). The turbulence intensity is significantly reduced near the LCFS and in higher GAM region.

3. 2. Dynamics of multiple sheared flows

Now we considered the multiple flow generation mechanism from turbulence via Reynolds stress. Figures 5 (a) and (b) show the radial distributions of the turbulence Reynolds stress and its gradient in Ohmic and ECRH plasmas, respectively. Here, the Reynolds stress and its gradient are estimated as $R_s = < v_r v_\theta >$ and $R_s^{'} = d < v_r v_\theta > / dr$, with v_θ and v_r being the poloidal and radial fluctuating velocities, respectively. The Reynolds stress has a maximum at Δr~-1.0 cm, where its gradient is close to zero and changes sign from positive to negative inward. The stress force is expressed as $dV_\theta / dt = -R_s^{'} - \gamma_d$, where γ_d is dissipation rate. The negative $R_s^{'}$ near the LCFS means that the mean flow develops there which is consistent with the measurement of Mach numbers. The Mach numbers have maximums at Δr~-1.0 cm, and the positive and negative Reynolds stress forces near Δr~-1.0 cm are observed. The result suggests that the Reynolds stresses is correlated with the mean flows. The $R_s^{'}$ profile is similar to those of LFZF from Δr~-1.0 cm to -5 cm and inverses with that of the mean flow. The correlation between GAM and stress is not observed in this analysis since the GAM has a finite frequency.

The correlation between the GAM and the turbulence stress is explored further in Ohmic plasmas. Figure 6 (a) and (b) show the power spectra of turbulence stress gradient R_s' and the radial electric field fluctuations E_r at the radial position of Δr~-3.0cm, respectively. The peak at the GAM frequency of ~7 kHz is observed in Figures 6 (a) and (b). Figure 6 (c) gives the

coherency spectra between the turbulence stress gradient and the radial electric field fluctuations. The coherency in GAM frequency band is about 0.5 which is quite high. This indicates that the stress gradient is well correlated with the GAM flow. Their phase shifts are also calculated and given in Figure 6 (d). The phase shifts of the GAM flow and the stress gradient are close to $\pi/2$, with GAM lagging the stress gradient. This suggests that the stress indeed drives the GAM.

3.3. Effects of multiple sheared flows on turbulence

The modulation effects of the flow shear on the turbulence are worth exploration for the LFZFs and GAMs. Figure 7 (a) shows the time evolutions of the LFZF shearing rate $V_\theta^{'}$ (the light line) and turbulence energy in LFZF frequency band $\phi^2 - \langle\phi\rangle^2$ (the heavy line) at the position of Δr~-1.2cm in ECRH plasma with heating power of ~700 kW. Here, the potential fluctuations at three radial positions are used to estimate the shearing rate and the potentials at the midpoint of them are selected to evaluate the turbulence energy. The LFZF shearing rate is found to be well correlated with the turbulence energy. Their phase shifts are all close to $\pi/2$. The similarity of this correlation property between GAM shearing rate and turbulence energy in GAM frequency band is shown again in Figure 7 (b). This observation suggests that the turbulence is modulated by both the LFZF and GAM.

The effects of sheared flows on the particle flux induced by turbulence in the frequency band of 15-500 kHz are measured by fast movement probes in Ohmic plasma. Figure 8 shows the radial profiles of particle flux, In this discharge, the safety factor is q_{95}=4.0. The particles flux slowly increases first from the far SOL to Δr~1cm, then decreases inward and gets to the minimum at the LCFS. Inside the LCFS, it sharply increases again from Δr~0cm to -1cm, then the flux drops again in the GAM peaking region (Δr~-2cm). The results suggest that the mean flows and GAMs suppress the particle flux induced by the turbulence. The particle flux is being measured by the probe at a single point, while generalizations are being made about total particle flux and correlation to amplitude of GAMs and LFZFs, which should be n=0, m=0 structures and thus influencing flux over entire magnetic flux surface. Furthermore, the minimum of particle flux at the LCFS is not consistent: GAMs and LFZFs are probably small

to non-existent here and measurements on other experiments have suggested there are large particle fluxes at the LCFS.

3.4. Envelope modulation of LFZFs and GAMs

The interaction between the ZFs and turbulence, especially the effect of the former on the latter, is a key issue in the study of transport in magnetized plasmas. The interaction can in general manifest as turbulence envelope (TE) modulation by ZFs, and, in particular, by GAMs. We now consider the relation between the ZFs and TE. Figure 9 (a) shows the temporal evolutions of the LFZF and the TE in the LFZF frequency band of 0.5-4kHz in Ohmic plasma. One can see a clear anti-phase correlation between them. The TE was evaluated by Hilbert transform from the high frequency turbulence of 300 kHz< f<500 kHz and then band-pass filtered for the LFZF frequency range 0.5-4kHz. The negative values of the TE indicate that the turbulence intensity is below the average values. Shown in Figures 9 (b) and (c) are the auto-power spectra of the TE, the coherence and the phase between the ZFs and the TEs. The high power fraction, coherence up to ~0.6, as well as the phase shift of $\sim\pi$ confirms (statistically) the strong anti-phase correlation between the ZFs and TE. In addition, the coherence and the phase shift between the ZFs (GAMs) and the TEs of different frequency bands are plotted in Figure 9 (d) and (e) as functions of the central frequency of the band. Here, the band width is 50 kHz. The significant local coherence between the ZFs and AT modulation implies that the latter must be caused by the former. The increase of the coherency with the frequency and the invariance of the cross phase of π may indicate that the TEs in the different band ranges are all modulated by the ZFs, and the modulation is stronger for higher frequency fluctuations.

3.5. Spatial structures of turbulent envelopes

The spatial property of the TEs is investigated using the coherence between the potentials at two distant positions. Here, the selected frequency band of turbulence is from 300 to 500 kHz for evaluating the envelopes since the nonlinear coupling between ZFs and ATs in this frequency band range, observed from the correlation analyses between turbulence envelopes and flows as shown in Figure 9 (d), is stronger than that of the others. Figures 10 (a) and (b)

show the coherence and phase shift between the envelopes at two positions separated in the poloidal and toroidal directions. The significant coherence (higher than 0.2) and very low phase shift (m~ 0.34±0.02 and n~0.1±0.1) show the symmetric property of the turbulence modulation. The two-point correlation technique is used again to evaluate the radial scale of the TEs. As shown in Fig. 10 (c), the radial wave-number frequency spectrum $S_{env}(k_r, f)$ for TE is very similar to that of the floating potential itself [14]. As confirmation, Figures 10 (d) and (e) provide a comparison of the radial wave number spectra at the frequencies of the LFZF and GAM versus that of the TEs. The good agreement implies that the spatial characteristics of the TEs are similar to that of the LFZF and GAM. This result provides evidence that the modulation effects are caused by the interaction between the ZFs and the turbulence.

The spatial property of the TEs is also studied in GAM dominant case. The poloidal and toroidal symmetries of TE at the GAM frequency are consistent with the results when GAMs coexist with LFZFs. The radial wave-number frequency spectra of the TE, $S(k_r, f)$ are investigated more in detail and shown in Figures 11 (a)-(e) in various frequency bands. The finite radial wave numbers and the linear dispersion relations of the TE are clearly demonstrated in all frequency bands. The radial wave-number frequency spectrum $S_{env}(k_r, f)$ for TE shown in Figure 11 (f) is also very similar to that of the floating potentials.

4. Conclusion

The spatial structures of multiple sheared flow populations and fluctuations were simultaneously measured using combinations of Langmuir probe arrays in the edge plasmas of the HL-2A tokamak, with ohmic and ECRH heating. The peaking region of the GAMs locates at ~2-3 cm inside the LCFS. The LFZF and GAM tend to coexist in the inner region. The amplitude developments of the multiple sheared flows and turbulence with ECRH heating power are also investigated. The measurements of the profiles of turbulence Reynolds stresses and poloidal mach numbers show correlation between the stresses and mean flows which is consistent with the theory that plasma poloidal rotation is driven by turbulence nonlinear interaction, via the stresses. The correlation between GAMs and oscillatory turbulence stresses is also observed. The turbulence is modulated at frequency of the multiple

sheared flows simultaneously and the particle fluxes induced by turbulence are significantly suppressed near the last close flux surface and in the GAM peaking region. In addition, envelope analysis shows that LFZFs and GAMs modulate turbulence and the spatial structures of the turbulent envelopes at the LFZF and GAM frequency are similar to those observed in LFZF and GAM.

This work is supported by the WCI Program of the National Research Foundation of Korea funded by the Ministry of Education, Science and Technology of Korea [WCI 2009-001], NSFC Grant Nos. 10775044, 11175060, 91130031 and 11075046, the National Magnetic Confinement Fusion Science Program Grant (2010GB106001 and 2010GB106008), the National Basic Research Programme of China under Grant Nos. 2008CB717806 and 2009GB105005, the U.S. Department of Energy (DOE) under Award Number DE-FG02-04ER54738 and CMTFO, and Fundamental Research funds for Central Universities, China-Korean joint foundation under the Grant No. 2012DFG02230.

Reference

[1] Biglari, H. et al., Phys. Fluids, **B2**, 1 (1990).

[2] Diamond, P. H. et al., Plasma Phys. Cont. Fusion, **47**, R35(2005).

[3] Itoh, K and Itoh. S. I, Phys. Plasmas 13, 055502 (2006).

[4] Diamond, P. H. et al., Phys. Rev. Lett. **72**, 2565 (1994).

[5] Miki. K and Diamond. P. H, Phys. Plasmas, **17**, 032309 (2010).

[6] Galperin. B, and Sukoriansky. S, Phys. Soc , **132**, 014034 (2008).

[7] Hasegawa. A et al., Phys. Rev. Lett. **59**, 1581 (1987).

[8] Chen. L et al., Phys. Plasmas, **7**, 3129 (2000).

[9] Winsor. N et al., Phys. Fluids, **11**, 2448 (1968).

[10] McKee. G. R et al., Phys. Plasmas, **10**, 1712 (2003).

[11] Zhao. K. J et al., Phys. Rev. Lett. **96**, 255004 (2006).

[12] Fujisawa. A et al., Phys. Rev. Lett. **93**, 165002 (2004).

[13] Gupta. D. K et al., Phys. Rev. Lett. **97**, 125002 (2006).

[14] Zhao. K. J et al., Plasma Phys. Cont. Fusion **52**, 124008 (2010).

[15] Liu. A. D et al., Phys. Rev. Lett. **103**, 095002 (2009).

[16] Pedrosa. M. A , et al., Phys. Rev. Lett. **100**,215003 (2008).

[17] Coda. S, et al., Phys. Rev. Lett. **86**, 4835 (2000).

[18] Moyer. R. A, et al., Phys. Rev. Lett. **87**, 135001 (2001).

[19] Ido. T et al., Plasma Phys. Cont. Fusion **48** S41 (2006).

[20] Nagashima. Y et al., Plasma Phys. Cont. Fusion **49**, 1611(2007).

[21] Zhao. K. J et al., Phys. plasmas **14**, 122301 (2007).

[22] Lan. T et al., Phys. plasmas **15**, 056105 (2008)

[23] Kim. Y. C et al., IEEE Trans. Plasma Sci. **7**, 120 (1979).

[24] Holland. C et al., Phys. Plasmas **14**, 056112 (2007).

[25] Xu. M et al., Phys. Rev. Lett. **108**, 245001 (2012)

[26] Hidalgo. C et al., Phys. Rev.Lett. **83**,2203 (1999)

[27] Holland. C et al., Phys. Rev. Lett. **96**, 075004 (2006).

[28] Tynan. G et al., Plasma Physics Control Fusion, **48** S51 (2006).

[29] Shafer. M. W et al., Phys. Rev. Lett. **103**, 075004 (2009)

[30] McKee. G. R et al., Nucl. Fusion, **49**, 115016 (2009).

[31] Schmitz. L et al., Nucl. Fusion 49, 095004 (2009).

[32] Xu. G. S et al., Phys. Rev. Lett. 107, 125001 (2011).

[33] Hidalgo. C, Plasma Phys. Control. Fusion 53, 074003 (2011).

[34] Estrada. T et al., Europhys. Lett. 92, 35001 (2010).

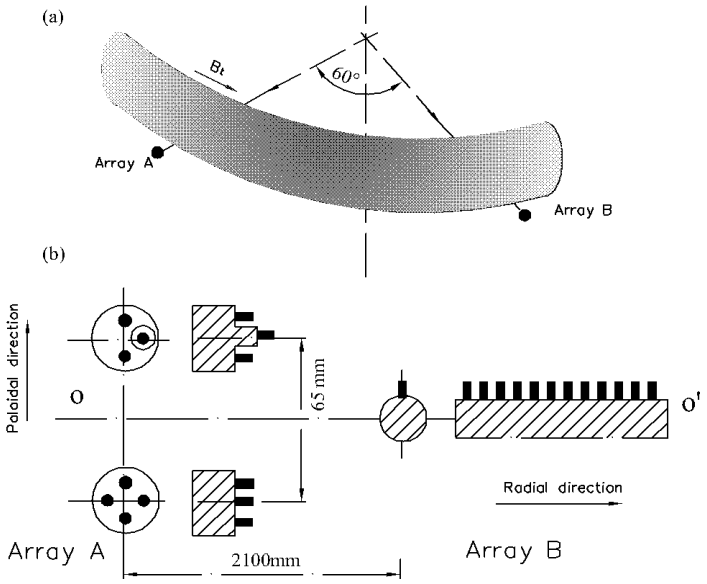

Fig. 1. (color online) Layout and structure of the LP arrays.

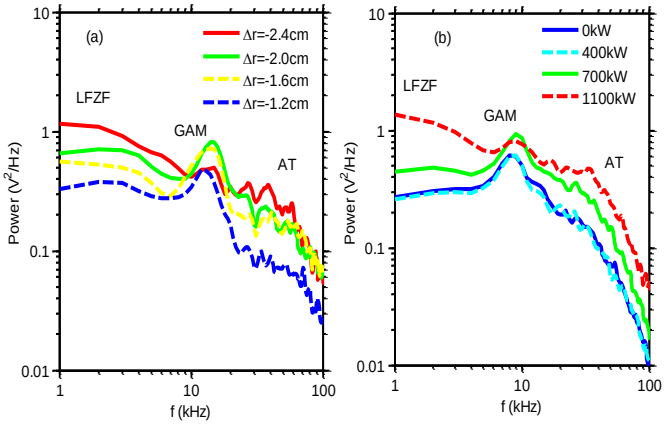

Fig.2. (color online) (a) Typical auto-power spectra of floating potentials at the radial positions of Δr=-2.4, -2.0, -1.6, and -1.2 cm in ohmic plasma, where the minus sign means inwards from the LCFS, (b) potential power spectra at ~-1.2cm with ECRH power of 0, 400, 700, and 1100 kW.

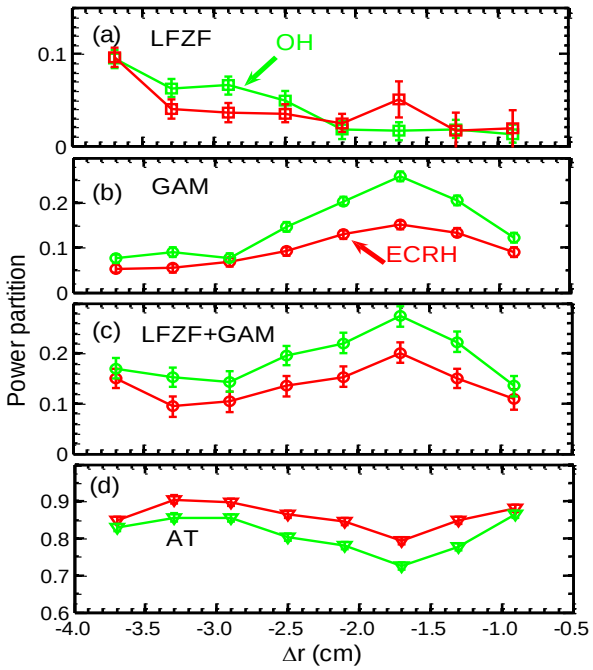

Fig. 3. (color online) The radial distributions of power partitions of the LFZF (a), the GAM (b), the LFZF+GAM (c), and the AT (d) in ohmic and ECRH plasmas. (I_p=150kA, q_{95}=4.0, N_e=1×10^{13}cm^{-3})

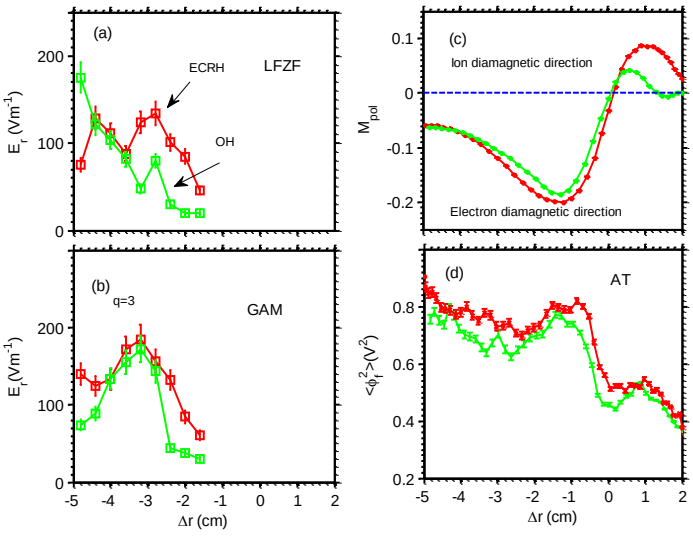

Fig. 4. (color online) The radial profiles of LFZF (a) and GAM (b) electric field, and poloidal Mach number (c), turbulent power (d). (Ip~170kA, q_{95}~3.2, N_e~1×10^{13}cm^{-3})

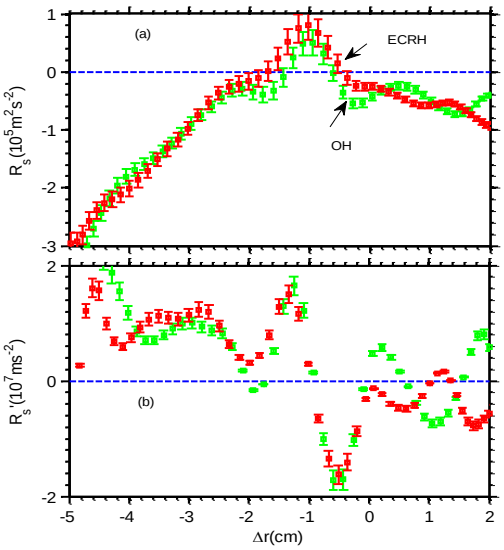

Fig. 5 . (a) Turbulent Reynolds stress and (b) its gradient.
(Ip~170kA, q_{95}~3.2, N_e~$1\times10^{13}cm^{-3}$)

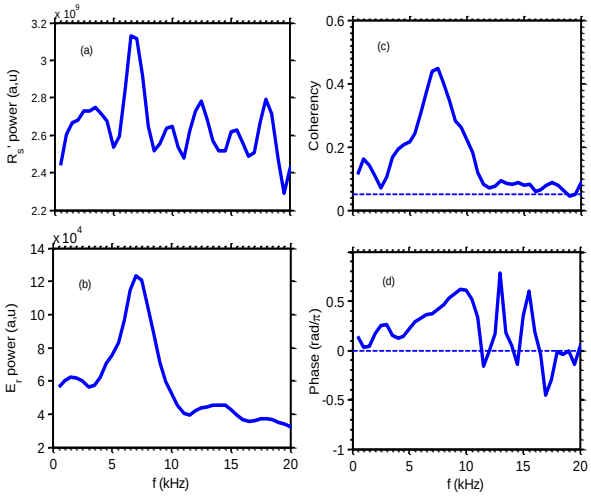

Fig. 6. (color online) The power spectra of the Reynolds stress gradient (a) and the radial electric field fluctuations (b), the coherency spectra between the stress gradient and the radial electric field fluctuations (c), and their phase shifts (d). (I_P~300kA, q_{95}=4.3, N_e=$3\times10^{13}cm^{-3}$)

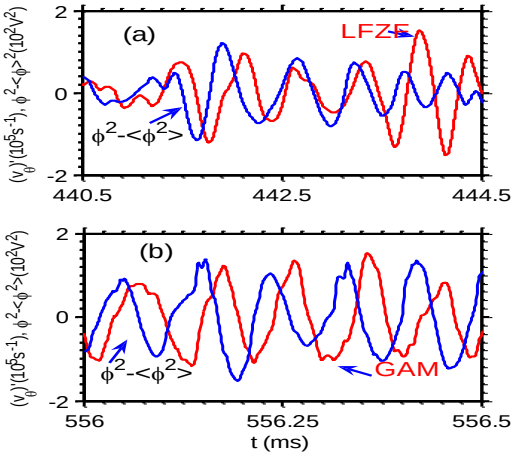

Fig. 7. (color online) (a) The shearing rate of LFZF and the $\phi^2 - \langle\phi\rangle^2$ in LFZF frequency band, (b) the shearing rate of GAM and the $\phi^2 - \langle\phi\rangle^2$ in GAM frequency band. (I_p=150kA, q_{95}=4.0, N_e=1×10^{13}cm^{-3}, P_{ECRH}=500kW)

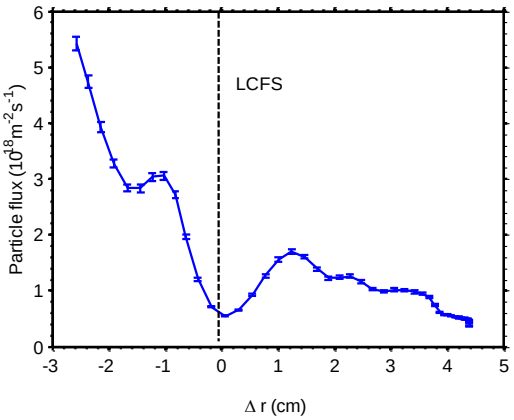

Fig. 8. (color online) The profile of particle flux induced by turbulence. (I_p=150kA, q_{95}=4.0, N_e=1×10^{13}cm^{-3})

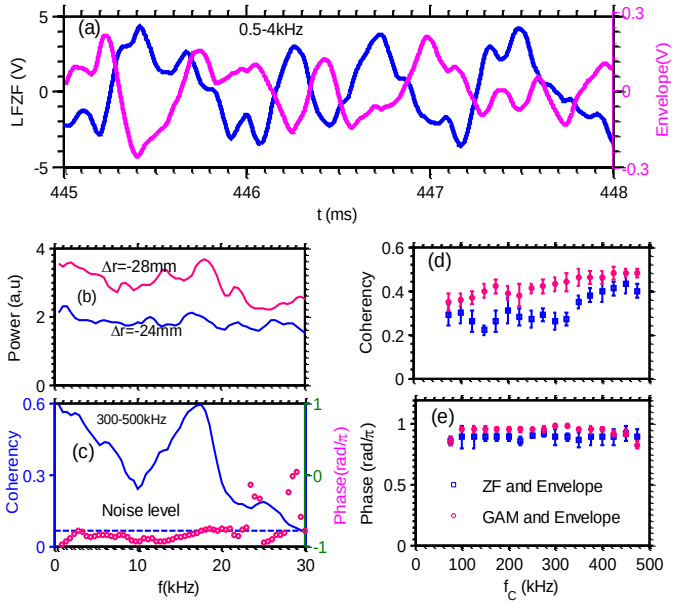

Fig. 9. (color online) (a) Waveforms of the LFZF and TEs, (b) the auto-power spectra of the TEs evaluated for the frequency band from 300 to 500 kHz, at two radial positions, (c) the coherency and cross phase spectra between the floating potentials and the TEs, (d) coherence and (e) cross phase between zonal flows (LFZF and GAM) and TE versus the central frequency of the band. (I_p=150kA, q_{95}=3.6, N_e=1×$10^{13}$$cm^{-3}$)

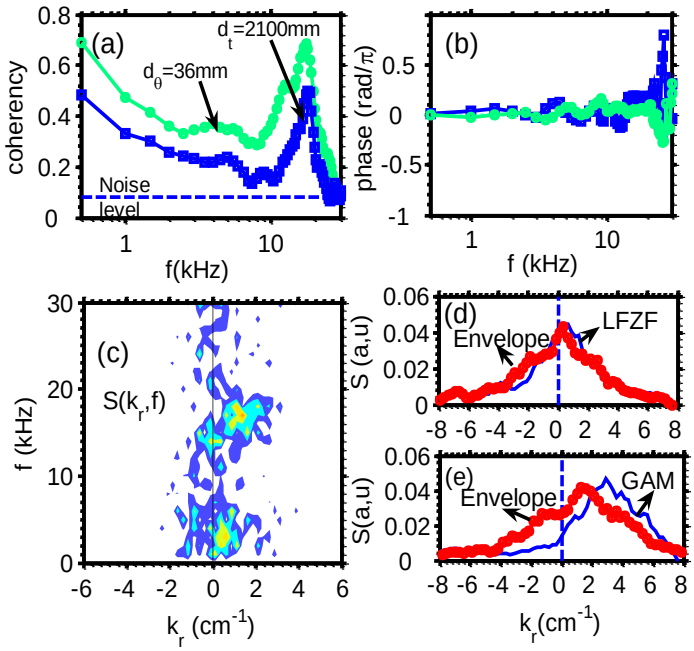

Fig. 10. (color online) (a) Poloidal and toroidal coherence between TEs (the light and dark lines) at the two same positions as those in Fig.~2, (b) corresponding cross phase. (c) Radial wavenumber frequency spectrum of the TE $S(k_r,f)$. (d) The radial wavenumber spectra of the floating potential and the TE for the LFZF, and (e) that for the GAM in Ohmic plasma (I_p=150kA, q_{95}=3.6, $N_e=1\times10^{13}cm^{-3}$).

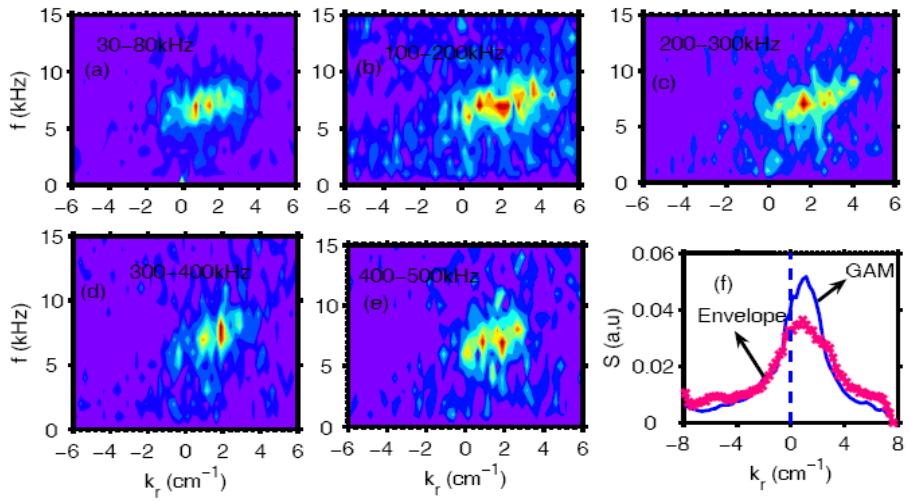

Fig. 11. (color online) (a)-(e) Radial wavenumber frequency spectrum of the TE $S(k_r,f)$ in various frequency bands in GAM dominant case, (f) the radial wavenumber spectra of the floating potential and the TE for the GAM in Ohmic plasma (I_P~300kA, q_{95}=4.3, N_e=2.5×$10^{13}$$cm^{-3}$).